Conformal Imaging with a Non-Contacting Microwave Antenna Array

Dun Li, Paul M. Meaney, Keith D. Paulsen

Thayer School of Engineering, Dartmouth College, Hanover, NH 03755 USA

***Abstract* — A model-based, non-contacting microwave imaging system, which allows for an arbitrarily shaped imaging domain to exist within the antenna array, has been developed using our Gauss-Newton iterative image reconstruction approach based on a hybrid of the finite element (FE) and boundary element (BE) methods. A new feature has been introduced to conform to the reconstructed field of view exactly to the coupling medium/object interface. This facilitates deployment of the reconstruction parameters solely to the zone occupied by the object, potentially improving resolution. Enhancements using this technique have been demonstrated in both simulations and phantom experiments.**

I. Introduction

As part of an experimental breast imaging research program, a water-coupled, non-contacting antenna-based microwave imaging system has been developed in conjunction with NIR (near infrared imaging), EIT (electrical impedance topography) and MRE (magnetic resonance elastography) for breast cancer imaging at Dartmouth College. Initial exams of 5 patients reported by Meaney, et al.[1], currently extended to more than 20 subjects, have successfully demonstrated that recovery of breast electrical properties at microwave frequencies is possible. This technique may possess significant advantages over conventional x-ray mammography, especially because of the high electrical property contrast between tumor and normal tissues at microwave frequencies [2].

The Gauss-Newton iterative approach is highly dependent on the match between the numerical model used for the forward solution and the actual measurement configuration. The existing forward algorithm divides the modeling task into two natural partitions: the heterogeneous imaging zone and the homogeneous surrounding region with their interface being somewhat arbitrarily defined. The solution from each zone is subsequently coupled together to complete a full forward solution. For general purposes imaging, defining the field of view as the full concentric space within the circular antenna array is appropriate. However, for site-specific applications such as breast imaging, it may prove useful to conform the interface between the two zones to the exact perimeter of the breast. While this approach requires two steps – defining the imaging object boundary within the non-contacting antenna array and reconstructing the image once the conformal boundary about the target has been defined, this paper will only examine the feasibility of the latter. Simulation and phantom experimental results are presented to demonstrate the potential benefits.

II. Overview of System

A. *Hardware System*

A clinical prototype microwave breast imaging system (Figure 1) has been implemented in Meaney et al. [1].

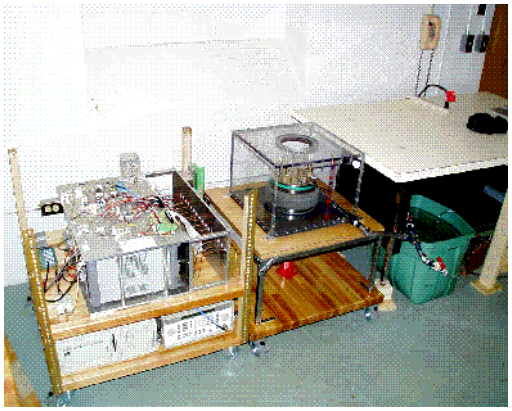

Fig. 1. Shows the partially assembled prototype imaging system with the electronics cart to the left coupled to illumination tank section to the right.

The electronics have been consolidated onto a single cart, which is coupled to an illumination chamber containing the inverted sixteen monopole antenna array that doubles as a section of the patient bed. The system has been designed for each channel to operate in either transmit or receive mode. It sequentially selects one monopole antenna at a time as the transmitter and nine opposing elements as

0-7803-6540-2/01/$10.00 (C) 2001 IEEE

receivers for measuring the TM electric fields. Both amplitude and phase information are recorded with high fidelity (>130dB signal to noise ratio) over a broad bandwidth (300MHz – 1.0 GHz). The antenna array is immersed in a 0.9% solution for the purpose of optimal signal coupling with biological targets and can be moved vertically with a hydraulic positioner, so that the breast can be illuminated at multiple vertical positions.

B. Image Reconstruction Scheme

Our microwave image reconstruction technique is a Gauss-Newton iterative scheme which minimizes the least squared error between the measured and computed TM electric fields to recover both the relative electric permittivity and electric conductivity distributions of the imaging object [3]. The forward solution of the electric field problem is governed by the Helmholtz equation and is unbounded, thus requiring representation of the fields in the surrounding medium. We accomplish this by utilizing a hybrid of the finite and boundary element methods [4]. The FE method is used to represent the imaging zone since it can accurately model an arbitrary heterogeneous region. The BE method is used to efficiently represent the surrounding homogeneous region since it only requires discretization of the boundary between the two zones. This approach eliminates the need for approximate boundary conditions. In addition, the source antennas are also positioned in the BE region where all electrical properties and sources remain constant during the reconstruction process. The actual reconstructed image is recovered on a dual mesh which is exactly superimposed over the mesh of the FE zone and is less densely discretized to significantly reduce the number of reconstruction parameters [5]. Figure 2a shows a general imaging case, in which a fixed FE mesh is placed concentrically within the antenna array representing the imaging domain containing a target (homogenous object with an inclusion) and surrounding saline.

An important feature of this overall model is that the actual FE mesh and associated dual mesh can assume any shape and position within the antenna array. As long as we can guarantee that the zone outside its perimeter contains only saline and no portion of the imaging object, this partitioning of the modeling region into two zones represented by the BE and FE methods, respectively, will produce an accurate solution. The FE mesh perimeter will correspond exactly with the object boundary in the ideal situation (Figure 2b). In this way the reconstruction parameters will be used for recovery of only the object properties and not an arbitrary blending with the surrounding saline. This essentially maximizes the number of parameter nodes used to represent the object, which is extremely important for image enhancement considering that the number of unknowns cannot be increased arbitrarily without also increasing the amount of measurement data. With the conformal domain, the algorithm allows for a step property change in the forward model at the coupling medium/object interface, which is precisely the situation that occurs with the measurement system when imaging the breast. Finally, if this concept is successful, we may also be able to improve the correlation analysis procedure with images from the NIR and EIT systems. These modalities illuminate the tissue via direct contact of optical fibers or electrodes, respectively, and do not require modeling of the surrounding medium. Since the recovered property distributions from those systems represent only the area

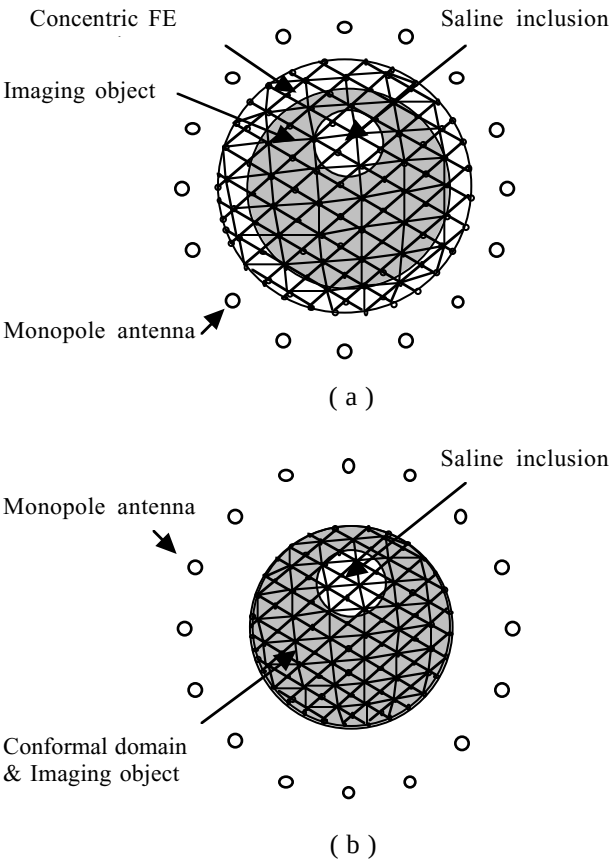

Fig. 2. Parameter reconstruction meshes with respect to antenna array. (a) Concentric FE mesh with an imaging object positioned within the antenna array. (b) Conformal FE mesh superimposed over the object.

0-7803-6540-2/01/$10.00 (C) 2001 IEEE

containing the breast, it will be easier to compare results with the microwave images using the conformal imaging domain technique than with the original antenna-concentric perimeter mesh.

III. RESULTS

Experimental evaluation of the new approach described in previous section is carried out in a numerical simulation and phantom test. Results compare images between the previous fixed mesh approach and the new conformal domain.

A. Simulations

For these experiments, the background saline medium had relative dielectric constant, ε_r=77, and electrical conductivity, σ=1.8 s/m at 900 MHz. The diameter of the concentric imaging area is 13 cm. The imaging object is a centered 8.2 cm diameter circle with electrical properties of ε_r=35 and σ=0.7 s/m. To mimic detection of a tumor-like object within a breast, we have inserted a 1.9cm diameter inclusion with the electrical properties identical to the background medium and 2.3 cm offset from the center. Figure 3a and b show the recovered relative permittivity (top) and conductivity images (bottom) at 900 MHz for the cases with the general concentric mesh and the conformal domain mesh, respectively.

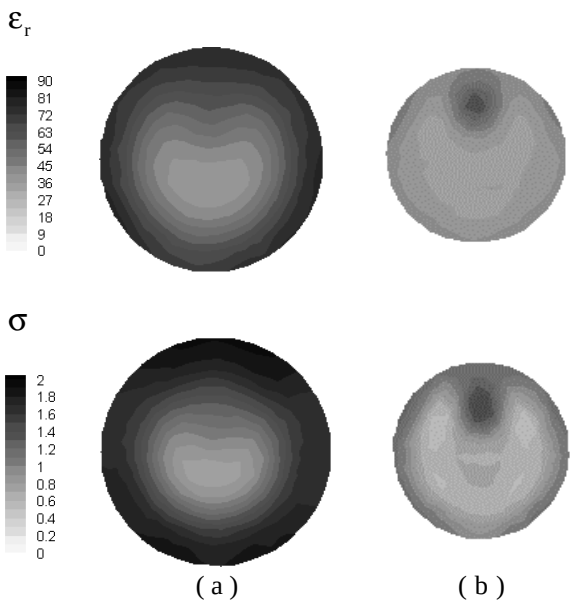

Fig.3. Reconstructed images of a simulated 8.2 cm diameter breast equivalent object with a 1.9 cm diameter tumor inclusion for two different FE meshes: (a) the concentric fixed FE mesh, and (b) the conformal FE mesh.

The images on the left recover the object with a gradual property gradient along the object/saline interface. The saline inclusion is only discernible as a minor indentation in the top of the object perimeter. The images using the conformal mesh present a uniform ε_r distribution over the breast except for the inclusion location where there is a significant property increase corresponding to the saline properties. The shape and size correlate well with the actual size. The conductivity counterpart demonstrates similar behavior with the inclusion size, shape and property value again being quite obvious.

B. Phantom Experiments

Phantom tests were performed with the imaging system described in Section II.A. In order to compare results with the simulation experiment, the phantom was constructed with the same size, shape, location and dielectric properties. The recipe for the phantom material is 78% syrup, 21% water and 1% agar. The saline used for the inclusion was the same as that of the coupling bath.

The results shown in Figure 4a and b are the recovered permittivity and conductivity images for the 8.2 cm diameter agar phantom with 1.9 cm diameter saline inclusion illuminated at 900 MHz using both the general concentric mesh and the conformal domain mesh, respectively. Similarly to the simulation experiment, the recovered images on the left (general concentric mesh) show the object with a gradual property gradient along the object/saline interface and the saline inclusion is only discernible as a minor indentation in the top of the object perimeter. The images using the conformal mesh present a more uniform ε_r distribution over the whole phantom except for the inclusion location where there is a localized property increase corresponding to the saline properties. The shape and size also correlate well with the actual size. The conductivity counterpart demonstrates similar behavior with the inclusion size, shape and property value again being quite obvious. The conductivity image appears to have minor artifacts that were not present in the simulation case. From past experience, we have noted that the recovered object size is often smaller in the conductivity versus the permittivity image. Thus, it is not unexpected that the conductivity image for the conformal mesh would show some darker zones around the perimeter corresponding to the higher conductivity associated with the surrounding saline. Additionally, it was not possible to exactly determine the location of the

agar phantom with respect to the antenna array. For the purposes of the images shown in Figure 4b, the location of the mesh was re-positioned empirically to reduce these artifacts caused by positioning errors.

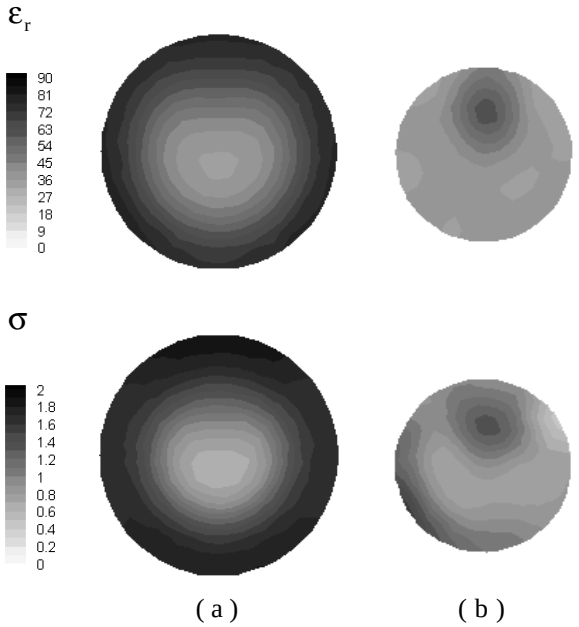

Fig.4. Reconstructed images of a 8.2 cm diameter biological equivalent phantom with a 1.9 cm diameter tumor inclusion for two different FE mesh. (a) Concentric fixed FE mesh. (b) Conformal FE mesh.

VI. Conclusion

Utilizing our model-based, hybrid element approach for image reconstruction, we have shown that it is possible to conform the imaging domain to the target tissue area. This technique allows us to deploy more nodes of the parameter reconstruction mesh to the region occupied by the object, potentially improving image resolution. It also allows us to apply a property step function at the object/coupling medium interface to accurately mimic the experimental configuration especially in cases where there is high contrast between coupling medium and object. It may also improve the ease with which the results from this imaging modality can be compared with others, specifically those such as EIT and NIR where the electrodes or fiber optic cables directly contact the tissue.

The results from this initial study using simple phantom and simulated cases with perfectly circular imaging objects has shown significant potential. More work needs to be done to determine whether these improvements will be observed for less uniformly shaped objects, and if so, whether robust and automated techniques can be developed to efficiently deduce an arbitrarily shaped object boundary.

Acknowledgement

This work was sponsored by NIH/NCI grant number PO1-CA80139-01.

References

[1] Meaney, P.M., Fanning, M.W., Li, D., Poplack, S.P., Paulsen, K.D., "A clinical prototype for active microwave imaging for the breast", *IEEE Transactions on Microwave Theory and Techniques*, Vol. 48, pp. 1841-1853, 2000.

[2] Chaudhary, S.S., Mishra R.K., Swarup A., Thomas J.M., "Dielectric properties of normal and malignant human breast tissues at radio wave and microwave frequency", Ind. J. Biochemistry Biophysics, Vol. 21, pp. 76-79, 1984.

[3] Seber G.A.F., Wild C.J., Nonlinear Regression, Wiley, New York, pp. 619-660, 1989.

[4] Meaney, P.M., Paulsen, K.D., Ryan, T.P., "Two-dimensional hybrid element image reconstruction for TM illumination", *IEEE Transactions on Antenna and Propagation*, Vol. 43, No. 3, pp. 239-247, 1995.

[5] Paulsen, K.D., Meaney, P.M., Moskowitz, M.J., Sullivan, J.M. Jr., "A dual mesh scheme for finite element based reconstruction algorithms", *IEEE Transactions on Medical Imaging*, Vol. 14, No.3, pp. 504-514, 1995.